



ISSN 1110-0451

## Arab Journal of Nuclear Sciences and Applications

Web site: [ajnsa.journals.ekb.eg](http://ajnsa.journals.ekb.eg)

(E S N S A)

### Synthesis Characterization and Gamma Irradiation Effect on Cobalt Doped ZnO Diluted Magnetic Semiconductor

Abdelhameed Sharaf\*<sup>1</sup>, A. Nasr<sup>1</sup> and Ahmed Aboud<sup>2</sup><sup>(1)</sup>Radiation Engineering Dept, National Centre for Radiation Research and Technology, EAEA, Cairo Egypt.<sup>(2)</sup>Department of Physics, Faculty of Science, Beni-Suef University, Beni-Suef 62514, Egypt.

#### ARTICLE INFO

Article history:

Received: 18<sup>th</sup> Nov. 2021Accepted: 5<sup>th</sup> Feb. 2022

Keywords:

Optical properties;

RTFM;

Diluted Magnetic Semiconductor;

ESR;

Spintronic.

#### ABSTRACT

In this manuscript, Cobalt (Co)-doped to Zinc Oxide (ZnO) samples prepared as thin films. These samples were obtained by utilizing spray pyrolysis have different concentrations of Cobalt. For investigating the effect of Co concentration on the thin films samples' physical properties, Different experimental techniques are employed. Such as Scanning Electron Microscope (SEM), X-ray diffraction, and optical spectroscopy. The grain size has been obtained using Scherrer's equation. From the obtained results, one can notice that the grain size behavior is non-linearly with the Co-concentration level. Electron Spin Resonance (ESR) is involved to observe the resonance absorption of microwave radiation of these thin films. It measures the spins of an electron of a molecule or an atom in a magnetic field. The study is performed before and after irradiation doses of 1 KGy and 3 KGy. The ESR signal shows the ferromagnetic response at room temperature which is improved after irradiation with Gamma-ray. The optical band gap of pure ZnO film was found to be 3.25 eV and the minimum bandgap is 3.11 for 1wt%. The existence of Co in the obtained film was confirmed by Energy Dispersive X-Ray (EDX) data. From the obtained results, the percentage of Co is increasing from 1.9% to 5.4% when the wt% is raising. In addition, the effect of the ionizing radiation doses; 1KGy and 3 KGy, on the magnetic and structural properties are investigated. As a result, Magnetic measurements for all prepared samples show a Room Temperature Ferromagnetic (RTFM) behaviour. Finally, increasing Co concentration and Gamma-ray irradiation dose will have a notified change on the ESR signal.

#### 1. INTRODUCTION

Minimizing the device dimensions gives improvements in microelectronics and magnetic data storage devices. Upcoming to nano scale, the design of materials parameters is forced to their perfect standards. Continued device miniaturization is becoming increasingly challenging. At this point, a common agreement that the present rate of miniaturization cannot be continued. As a result, new methodologies of device fabrication need to be established. The spintronic is one such methodology that is based on the use of charge and spins dynamics of electrons in certain multifunctional substances [1-5].

There is a diversity of novel device concepts which have been proposed based on this technology. The serious step in the operation of a spintronic device is to inject and detect of spin polarization carriers of the interface of the ferromagnetic semiconductor surface.

In spite of great efforts, effective injection of spins into nonmagnetic semiconductor stays to be a major difficulty in this field. Magnetic metals such as cobalt, nickel and iron were used in previous studies for injecting spin-polarized carriers into a semiconductor material. There are three diverse methods that have been proposed for the injection of spin polarization carriers into semiconductors effectively: tunneling spin-polarized carriers is one way of this method in which a ferromagnetic metal is injected into the semiconductor through an insulator [6, 7], and using dilute magnetic semiconductors (DMS) [8] which are ferromagnetic and whose conductivity can be tuned to match the nonmagnetic semiconducting transport medium.

ZnO is a wide bandgap semiconductor with high chemical stability and low-cost production which is found to have high catalytic efficiency. Studying the

effect of Pb, Ni, and Cu doping in the water splitting performance of ZnO thin films [9]. It shows that the incident applied bias efficiency and conversion efficiency of the photon-to-current were 30% at 390 nm and 0.636 at 0.5 V, respectively. In another work, the investigation of the water splitting and chemical stability of ZnO/titania, showed a 25% higher PEC water splitting activity than the as-deposited ZnO [10 -11].

Zinc oxide (ZnO) is one of the most important oxide transparent conductors (TCO) materials which is most attractive for different applications. Co-doped ZnO thin films may be a good candidate for suitable application in various optoelectronic devices such as the manufacture of solar cells. It is observed that pure ZnO shows a weak ferromagnetic nature whereas Co doped thin films exhibit good ferromagnetic properties, which is used in the field of spintronic applications [12- 14].

In this study, we report the effect of the Co doping level on the physical properties of ZnO thin films and the impact of this doping on the magnetic properties of the deposited films. The prepared thin films were obtained using the same deposition conditions with changing the concentration level of the Cobalt. Different techniques were used to investigate the physical properties of pure and cobalt doped zinc oxide. The electron spin resonance (ESR) is used which is an effective method for the observation of the absorbed microwave radiation by the spins of an electron of an atom or molecule in a magnetic field. Also determined by this technique valuable information about the lattice site in which ferromagnetic dopant ions are located

## 2. Experimental Techniques

All films studied in this work had been deposited using a spray pyrolysis technique. Spray pyrolysis involves a solution spread of a constant concentration onto a preheated substrate. The process takes place at a constant temperature. For this purpose, 5 gm of Zinc, acetate pentahydrate has been dissolved in a mixture of 30 ml Methanol and 30 ml distilled water. Keep stirring the solution for 20 min until it's all clear. The substrates were placed onto a stainless steel hot plate which was placed above a Ni-Cr wire of 20 K-Watt. This Ni-Cr wire was connected to a temperature controller Omega type to fix the temperature at 380°C. The variation of the controller temperature was found to be  $\pm 2$  from the mentioned temperature. Continuously this solution has been sprayed onto a glass substrate. The solution spray has been done at an air flow rate of 20 L/min. For doping calculated amounts of cobalt acetate penta hydrated have been used. The amount of Cobalt acetate was weighted to be 1, 5, and 10 weight % from the 6 grams of the zinc acetate used for the pure film. All films were taken

directly from the Holt plate after the solution was sprayed completely. Pure ZnO films were found to be transparent and in good adhesion to the substrate. Co-doped ZnO films were found to be green in colors and also in good adhesion to the glass substrates. No pinholes can be observed in any of the deposited films.

All deposited films were investigated with various techniques to diagnose the effect of Co-doping on the different properties of ZnO. X-ray diffraction investigation has been done using Philips equipment for Cu-K $\alpha$  of wavelength 1.54Å and 2 $\theta$  range 5-85 degrees. Morphology analysis as well as elemental analyses of the undoped and Co doped ZnO thin film samples were performed using (EDX), Energy-dispersive X-ray (EDX) spectroscopy with a scanning electron microscope. The crystalline phases of the obtained nanoparticles deposited on the glass substrate were identified using X-ray diffraction (XRD). The electromagnetic spin resonance (ESR) measurements were performed at room temperature. The Raman spectra of the prepared thin films were obtained by Raman spectroscopy. The optical absorbance measurements of the prepared samples were performed by using a double beam (Shimadzu UV-160A) spectrophotometer in the wavelength range 200– 1100 nm. A Cobalt-60 Gamma cell was used for irradiating the prepared thin film samples at 1 and 2 kGy as an accumulative dose of 1 and 3kGy.

## 3. RESULTS AND DISCUSSION

### 3.1. Energy Dispersive X-ray Spectroscopy (EDX)

Presented in Fig. 1 the spectra of the EDX for pure thin film samples as well as the cobalt (Co) doped thin film samples. The spectrum indicates that the cobalt ions were successfully merged in the zinc oxide matrix. Given in Table 1, the elemental analysis acquired from the EDX analyses.

**Table (1): presents the EDX composition analysis for pure ZnO and Co doped.**

Compound	Zn %		Co %		O <sub>2</sub> %	
	0KG	1KG	0KG	1KG	0KG	1KG
ZnO	98.7	99.5	-	-	1.3	0.5
ZnO:Co (1%)	98.1	98.8	1.9	0.9	0.0	0.2
ZnO:Co (5%)	96.8	95.9	3.2	4.1	0.0	0.0
ZnO:Co (10%)	94.6	93.3	5.4	6.7	0.0	0.0

It is clear from reading the data in Table 1 that there is no agreement with practical measurements. This return to the concentration of pure ZnO thin films which is about 50 % as shown in Fig. 1-a, [15] for each components. It is not seen in Table 1 and Fig. 1-b. This

is done because the EDX doesn't differentiate precisely between heavy and light elements. So, the concentration of zinc in pure film approaches 99% of the total contents. The figure gives a good indication of the Co concentration in the films without irradiation. After irradiation, the concentration of Co tends to increase due to the replacement of Co atoms with the  $O_2$  in thin films.

It is evident that the data in Fig. 1-b is not valuable. In addition, it gives a good insight into the replacement of oxygen atoms by cobalt atoms. Also, it is adopted with the SEM and XRD analysis which is given in the next two subsections.

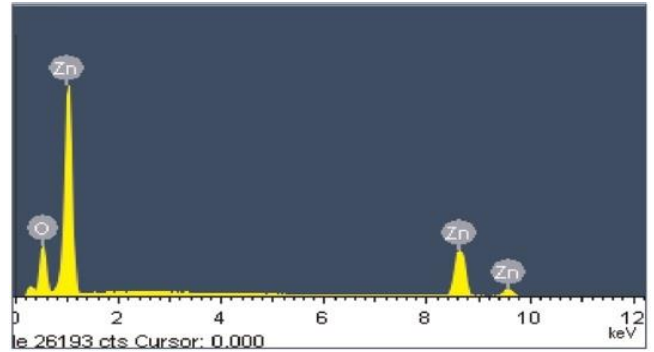


Fig. (1-a): EDX spectra of the synthesized ZnO:Mn nanoparticles [15].

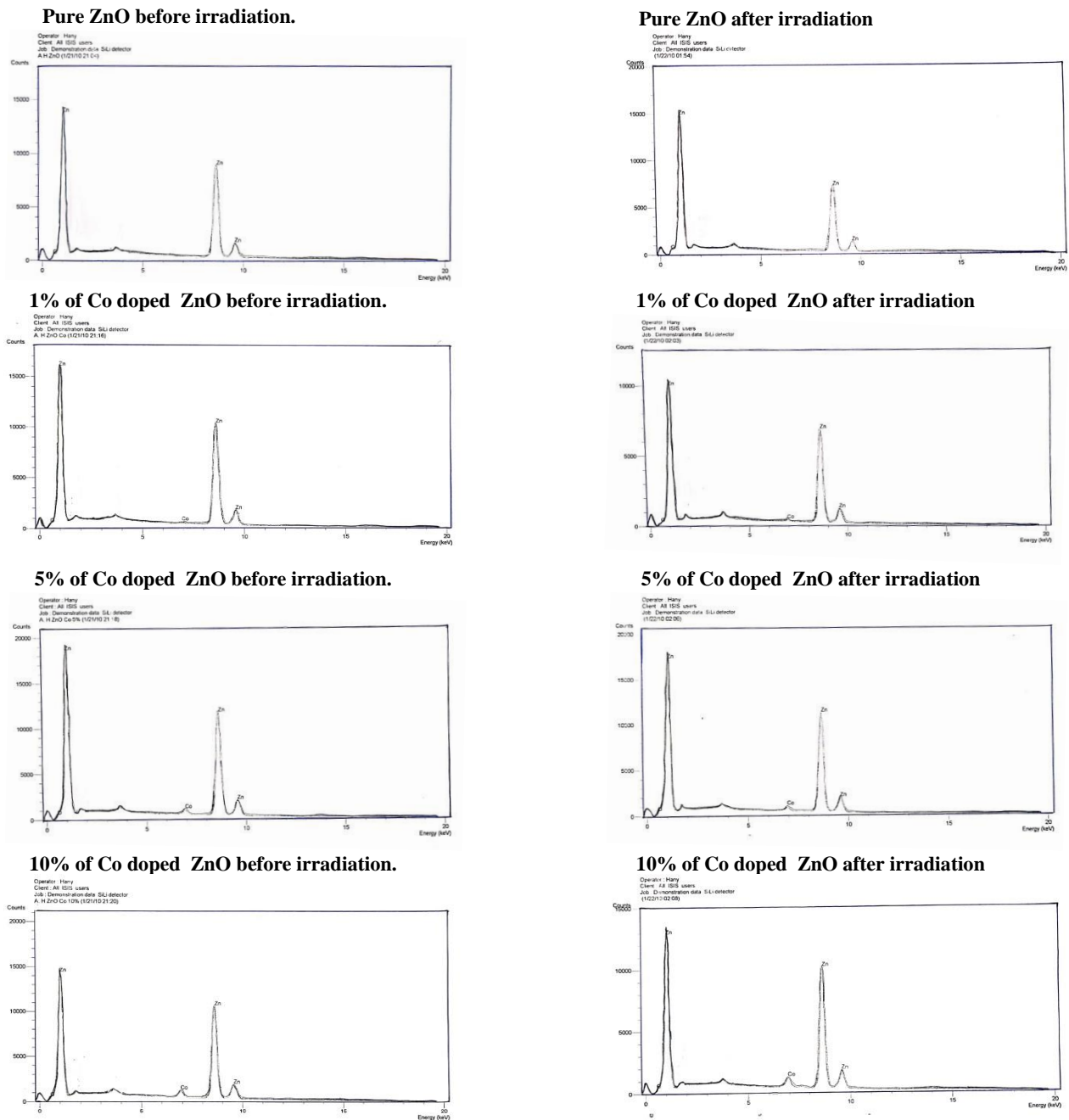
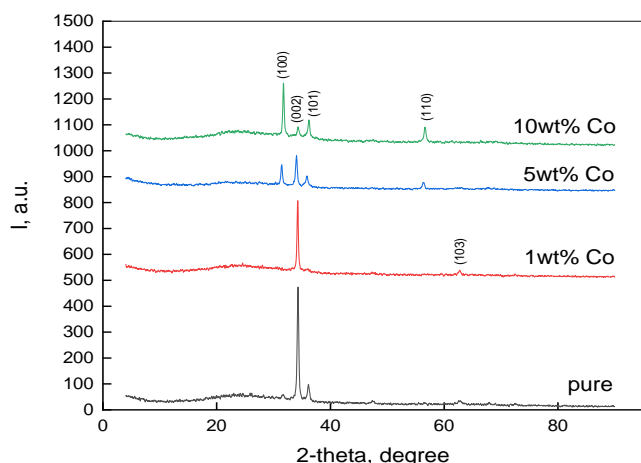


Fig. (1-b): EDX analysis; Left before radiation for concentration 0%, 1%, 5%, and 10% of Co respectively, and right after radiation for the corresponding concentrations.

### 3.2. The X-Ray Diffraction (XRD) Analysis

Presented in Fig.2 the X-ray diffraction patterns of all deposited films in the 2-theta range from 5 to 85 degrees. Two diffraction peaks have been located at  $2\theta$  of 34.244 and 36.085 degrees. These two peaks can be attributed to the hexagonal ZnO phase according to ICDD card number 79-0205. The first peak refers to (002) plane and the second are (101). Obtaining ZnO films with (002) as the main diffraction peak has been recorded with other authors using spray pyrolysis and other techniques [9, 11]. Films deposited from 1wt% concentration precursor shows two diffraction peak the highest belonging to (002) and the other to (103) plan. In this film, no peak for (101) is recorded. In another work of Karzaziwt al [16] ZnO films were found to preferably crystalline in the (103) plane.



**Fig. (2): Shows the X-ray diffraction patterns of all as-deposited thin films.**

Increasing the Co-content in the starting solution up to 5wt% of the deposited films will lead to a significant change where new diffraction peak at 31.78 degrees which belongs to the (100) plan. In the same film, the (101) starts to grow again. Finally, at the maximum concentration of Co of 10 wt%, (101) reflection becomes the maximum peak with a significant decrease in the (002) and (101) peaks intensities. It seems that increasing Co content in the deposited film changes the preferred orientation of the film from (002) to (100).

The growth of ZnO on amorphous substrates shows self-orientation behavior where the film can be oriented in an anisotropic fashion. Ohyama et al [17] studied ZnO thin films prepared from Zinc Acetate salt by utilizing the Sol-Gel technique. They recorded (002) as the

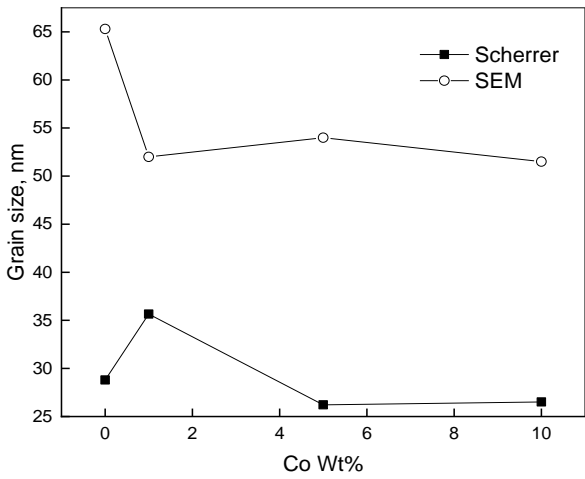
preferred orientation for all deposited films. Also in the work of Benramache et al [18] (002) orientation was found to be the preferred orientation for spray pyrolysis deposited ZnO thin films. Another work of Shukla et al [19] (100) was observed as the preferred orientation. These results said that ZnO grown on the amorphous substrate has a self-oriented behavior. The deposition techniques and deposition parameters seem to have a big influence on the preferred orientation. Novak et al [20] studied the effect of substrate temperature on the grown ZnO thin film. They found that the preferred orientation changes from (101), at low temperatures, to (002) at high temperature at 400°C as considered here. Doping processes also were found to play an important role in the preferred orientation of ZnO films on amorphous substrates. Changes in the preferred orientation upon Fe doping were recorded by Srinivasulu et al [21]. They found that at low Fe concentration (002) is the preferred orientation while at higher concentrations the preferred orientation changed to (101). Also, Al and Cu doping have the same effect of changing the preferred orientation [22-24]. Benramache et al [22] studied the effect of Co doping on the properties of ZnO thin film. These results revealed no change in the preferred orientation in the deposited films. Therefore, (002) plane stays the preferred plane at all Co concentrations up to 3 wt%. No change in the preferred orientation was recorded upon Co doping [23].

Generally, two types of orientation were recorded for ZnO thin films. One is the normal orientation which perpendicular to the film surfaces. The other is the parallel orientation which parallels the film surfaces. These changes in the preferred orientation of thin film grown on amorphous substrates may relate to changes in the nucleation process and growth mechanism[24-29]. In all films, no other diffraction peaks are detected which confirms the singularity of the ZnO phase.

Scherrer's equation [30] was used to calculate the average crystallite size of as-deposited films;

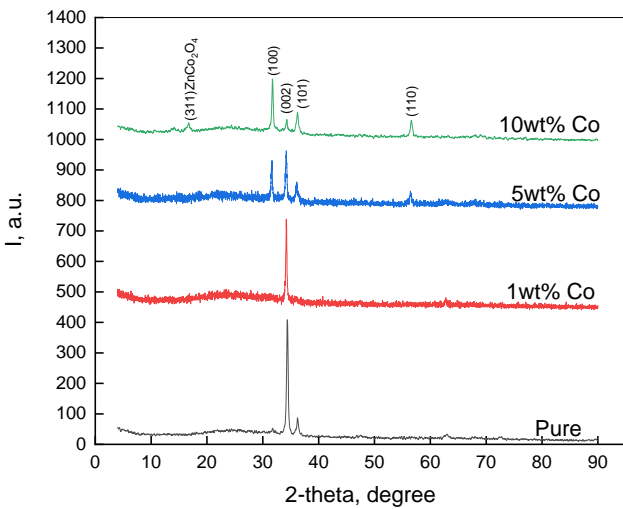
$$D = \frac{k\lambda}{\beta \cos \theta}$$

Where D is the average crystalline size,  $\lambda$  represents the radiation wavelength,  $\theta$  is the diffraction angle using the main peak information and  $\beta$  shows the full width at half maximum. Fig.3 shows the variation in the crystallite size obtained from Scherr's equation and SEM images.



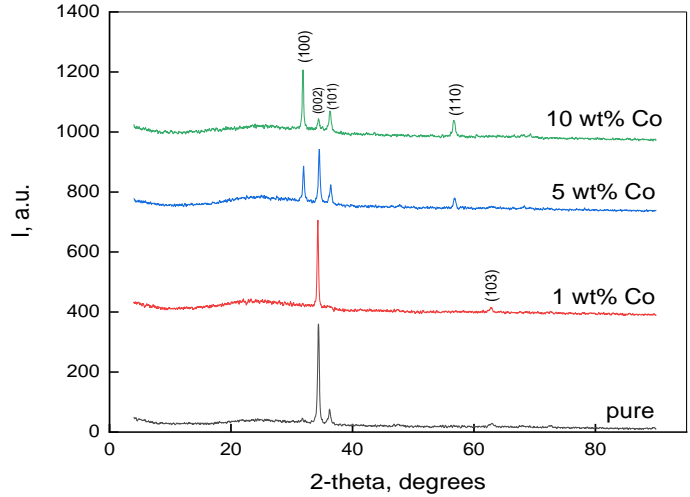
**Fig. (3): Crystallite size variation with Co content before and after variation.**

Figures 4 and 5 show the XRD After irradiation with gamma-ray at 1 and 3 KGy, respectively. Fig.4 shows the X-ray diffraction patterns of all films after 1 KGy dose of irradiation with Gamma. As shown in fig.5, the structure of the deposited films was changed by the irradiation, which has been summarized as follow; (1) pure film denotes the same two peaks, as in as-deposited films, (2) no (103) peak is recorded in the film with 1 wt%, (3) film deposited from 5 wt% precursor shows no change, finally, the new peak has been recorded at 2θ of 16.79 degrees which attributed to ZnCo<sub>2</sub>O<sub>4</sub> phase, ICDD card number 0-1149. It is worth noting here all recorded peak intensities are smaller than as-deposited film peaks intensities.



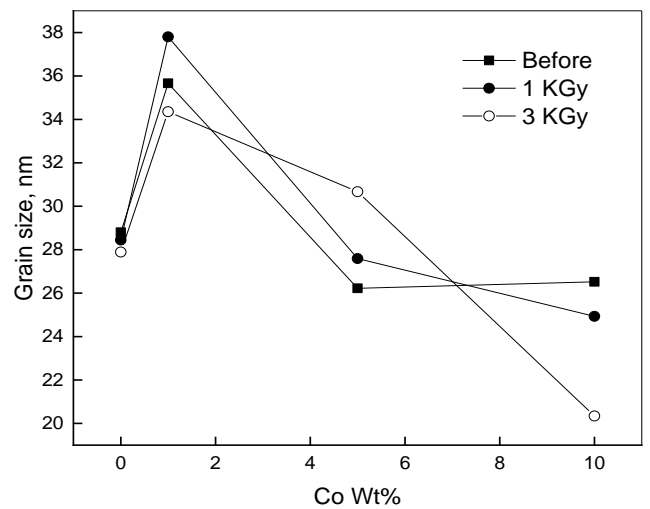
**Fig. (4): X-ray diffraction of all films after irradiation with 1 kGy.**

Fig.5 shows the XRD diffraction patterns for all films after the 3KGy irradiation dose. No significant changes are recorded except the disappearance of the ZnCo<sub>2</sub>O<sub>4</sub> peak at 16.79 degrees which recorded after 1 KGy.



**Fig. (5): XRD patterns for all films after 3KGy Gamma ray irradiation.**

Fig.6 shows the variation in the crystallite size for all films before and after irradiation with Gamma. One can notice that irradiation changes the behavior of crystallite size. It gives an arrangement order when the film with Co content around 5 wt%. in other contents the behavior is not stable. While decrease in the film with Co 10 wt%. The pure film shows an insignificant change after irradiation.



**Fig. (6): Crystallite size variation with Co content before and after variation.**

### 3.3. Scanning Electron Microscope

The effect of diverse fractions of Co concentrations on the surface morphologies of the thin films prepared was investigated from the SEM images as shown in Fig. 7.

Fig.7 shows the SEM images for all as-deposited films. As observed in the photos pure film shows clear grain size with different sizes. The average grain size as estimated from SEM imaging is 65.3 nm. Upon doping the film images show an attempt to agglomerate but

small grains are still observed. The grain size upon doping was estimated to be 52, 54, and 51.5 nm for 1, 5, and 10 wt% films, respectively. All recorded grain sizes are higher than what had been estimated using Scherer's equation. Also, the behavior is different where the grain size from Scherer's calculation increased after 1wt% doping, but from the SEM imaged it is found to decrease concerning the pure film. The SEM images of dope films also revealed the denser film is formed with higher surface roughness.

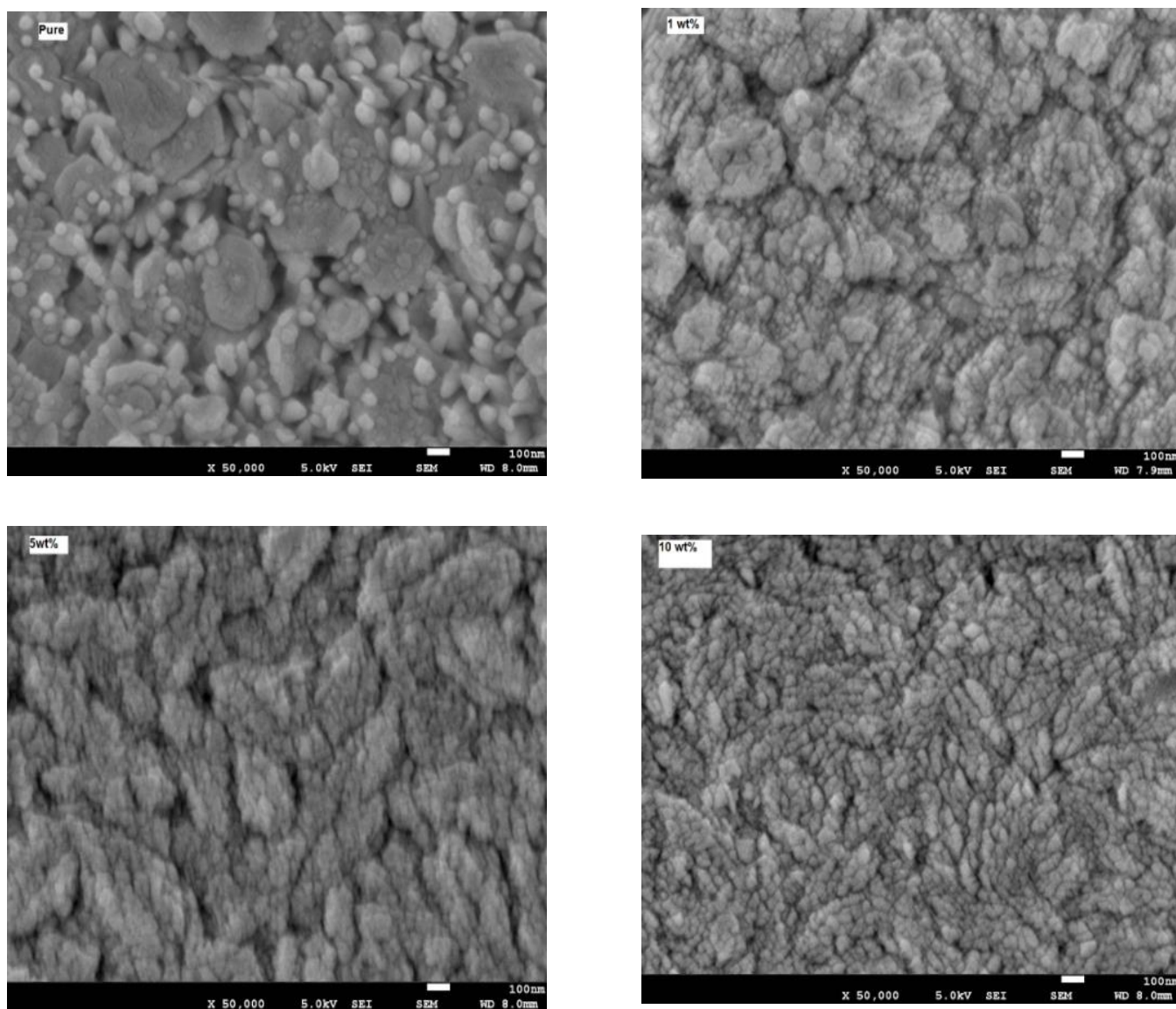


**Fig. (7): SEM images for all as deposited films at different Co-concentrations.**

### 3.4. Optical Band Gap

The optical transmission and reflection of all films had been recorded in the range of the spectral from 190 to 1100 nm. Fig.8 shows the transmission curve of Co 10wt% as an example of all deposited film transmission spectra. One can notice that the film indicates high transmission in wavelength range  $>400\text{nm}$ . Three absorption peaks are recorded at 562, 611, 658nm. These peaks are results of d-d transitions of  $\text{Co}^{2+}$  ions as charge-transfers between donor and acceptor ionization levels located within the bandgap of the ZnO host matrix[31-36]. They could be assigned to transition from  $4A_2 \rightarrow 2E$  (G),  $4A_2 \rightarrow 4T_1$  (P), and  $4A_2 \rightarrow 2A_1$ (G), respectively [37-42]. The existence of these absorption peaks vanishes the oscillation peaks that appeared at the beginning of the transmission spectra,  $\lambda > 800\text{nm}$  or  $\lambda < 800\text{nm}$ , please indicate. Such a spectrum with low fringes causes the transmission spectra to determine the thickness of the deposited films

not possible. Instead of that, the reflection spectra show a regular interference fringe and it can be used to determine the thickness of the films. Such an idea of using the reflection spectrum for determining the thickness of the films has been used by El-Naggar et al [43]. The thickness of all films was calculated using the Parav program [39]. The thickness was found to be 632, 1287, 955, and 840 nm for pure, 1wt%, 5wt%, and 10wt% films respectively. The band gaps for all films have been calculated according to Tauc's equation [9];

$$\alpha = A \frac{(hv - E_g)^n}{hv}$$

Here  $\alpha$  is the linear absorption coefficient, the photon energy,  $hv$ , the bandgap value  $E_g$ , and a constant  $A$ . Finally  $n$  is an exponent equal  $(\frac{1}{2})$  as a sign of the direct transition. The bandgap values were found to be 3.25, 3.11, 3.21, and 3.18 eV for pure, 1wt%, 5wt%, and 10wt% respectively.

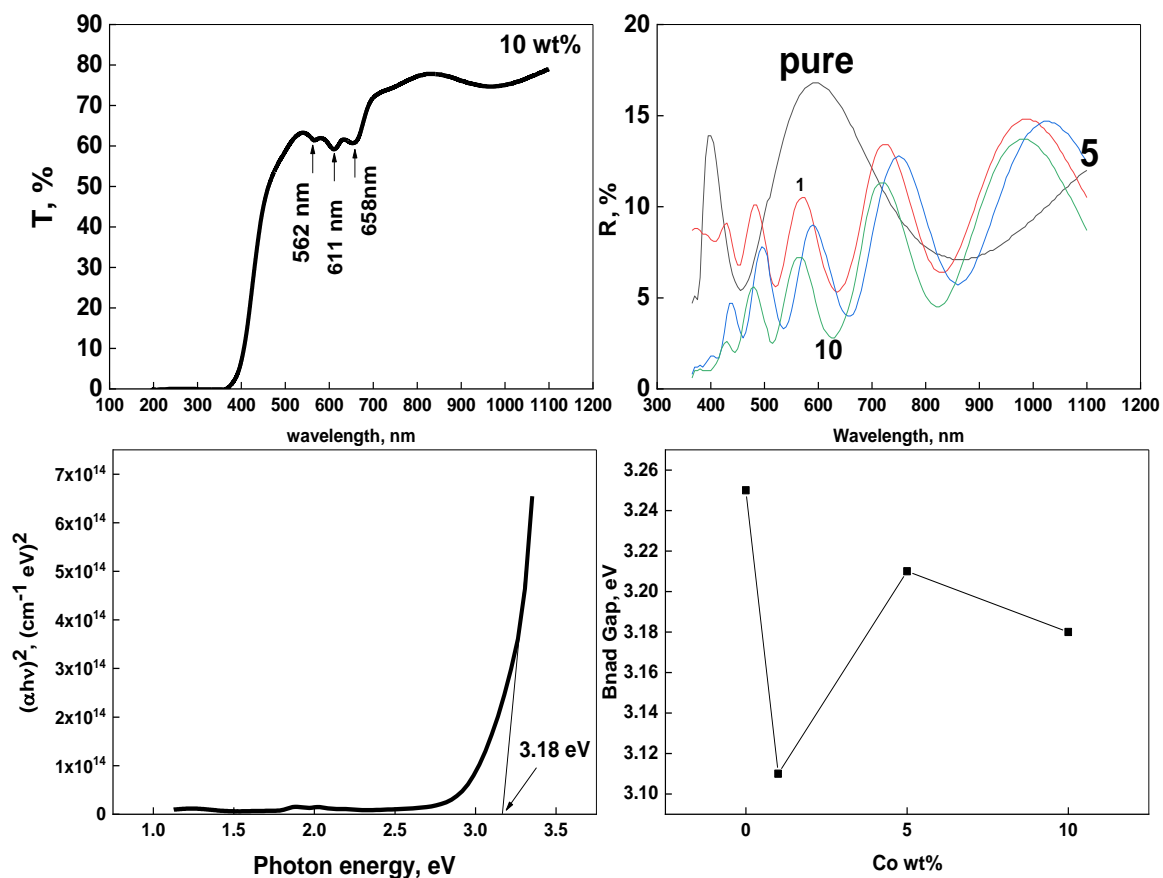


**Fig. (8): Optical Transmission of 10wt% film, Reflection of all films, Tauc's plot of 10wt% film, variation of the band gap and all films**

### 3.5. Electron Spin resonance

An effective method for the observation of the absorbed microwave radiation by the spins of an electron of an atom or molecule in a magnetic field is the Electron spin resonance (ESR) spectroscopy. Also determined by this technique a valuable information about the lattice site in which ferromagnetic dopant ions are located [44].

#### 3.5.1. Before Gamma Irradiation

The spectrum of the ESR for pure Zinc oxide and zinc oxide doped with cobalt nanoparticles thin films samples documented at room temperature are presented in Fig. 9 through Fig.12. It is clear that in ZnO doped with Co as a DMS, the dopant atoms have two opportunities. The first one is to occupy localized sites in the ZnO lattice- which leads to hyperfine splitting and appears of eight lines in the pattern of the ESR [45-48]. While the second opportunity is to form small clusters. In our case, as illustrated in Fig. 9 through Fig.12, the spectra of Co-doped ZnO samples studied gives a broad which indicates a room temperature ferromagnetism. The appearance of the broad signal in the ESR pattern due to the strong dipolar interactions between  $\text{Co}^{+2}$  ions. The electronic configuration of  $\text{Co}^{+2}$  ion is  $3d^7$ , and the electronic ground state is  $S_{7/2}$ , which splits into four Kramers doublets ( $\pm 7/2$ ,  $\pm 5/2$ ,  $\pm 3/2$ , and  $\pm 1/2$ ).

The Lorentzian functions were used to calculate the number of spins and the g-value related to each spectrum. All these values are tabulated in Table 2. The g-value for free-electron is  $g_e = 2.0023$  and the shift from this value is caused by the spin-orbit interaction of the electron in the atomic orbital [49]. The number of spins (*spin concentration*) ( $N$ ) of the considered samples can be determined from the following equation:

$$N = \frac{KH_o(\Delta H)^2(A/2)}{G_e H_m \sqrt{P_H}}$$

With the constant of the spectrum  $K \approx 9.1 \times 10^{12}$ ,  $H_o$  is the magnetic field measured in Gauss,  $\Delta H$  represents the width of the peak to peak magnetic field measured in

Gauss,  $A$  is the ESR signal intensity (*EPR signal peak height divided by sample weight*),  $G_e$  is the gain detection which is  $1.42 \times 10^4$ ,  $H_m$  is the modulation field which is 6 GGauss and  $P_H$  is the microwave power which is 5.041 mW. The number of spins,  $N$ , values are listed in Table 2. The concentration of paramagnetic defects has increased proportionally with the increase of Co doping in the ZnO and diminishes completely in the case of pure ZnO as a diamagnetic material.

**Table (2): The g-value, peak area of the ESR signal and the concentrations of the number of spins (N) of the ZnO and Co-doped ZnO**

Compound	g-value	Area	N(cm <sup>-3</sup> )
Pure ZnO	0	0	0
1% Co doped	2.01052	1115.9	1.89744E+17
5% Co doped	2.01056	1236.65	2.10276E+17
10% Co doped	2.01045	1437.536	2.44569E+17

#### 3.5.2. After Gamma Irradiation

All prepared samples are subjected to gamma-ray irradiation with 1KGy and 3KGy doses. Then the ESR is reinvestigated to the irradiated samples under the same condition before irradiation. Figures 6, through 9, show the ESR signal height (a.u.) (y-axis) for each sample before and after irradiation. It is clear from these figures the ESR signal increased linearly with the increase of the dose rate.

The increase in the ESR signal appears due to the effects of gamma irradiation which breaks bonds in the ZnO lattice which in turn leads to increasing in the free radicals. The paramagnetic defects values for the irradiated samples are listed in Table 3. It is clear from this table that it reflects brightly the increase in the ESR signal with the increase of both Co concentration and dose rate. It is shown that the paramagnetic defects increased in the case of 5% Co doping than 10% Co doping in case of 3KGy dose. This occurs as a result of as appearing a second new phase of CoO in which small clusters are formed as presented in the XRD analysis.

**Table (3): The g-value, peak area of the ESR signal and the concentrations of the paramagnetic defects (N) of the ZnO and Co-doped ZnO**

Gamma Dose	Compound	g-value	Area	N(cm <sup>-3</sup> )
1 Kgy	Pure ZnO	2.01626	638.6214	7.11193E+16
	1% Co doped	2.01504	3007.663	2.89584E+17
	5% Co doped	2.01509	3659.359	3.52331E+17
	10% Co doped	2.0151	3913.292	3.7678E+17
3 KGy	Pure ZnO	2.01641	2635.58	2.93337E+17
	1% Co doped	2.01516	6805.556	6.4666E+17
	5% Co doped	2.01515	8522.533	8.09807E+17
	10% Co doped	2.01515	8397.976	7.97971E+17

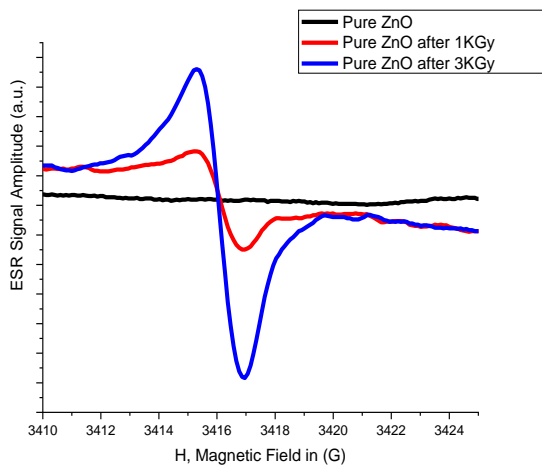


**Fig. (9):** ESR signal for pure ZnO samples before and after irradiated with 1KGy and 3KGy doses.

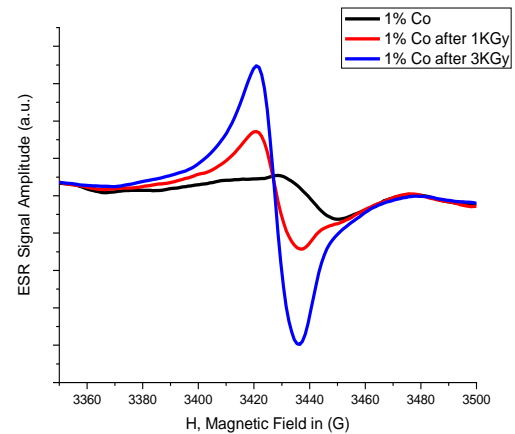


**Fig. (10):** ESR signal for 1% Co doped ZnO samples before and after irradiated with 1KGy and 3KGy doses.

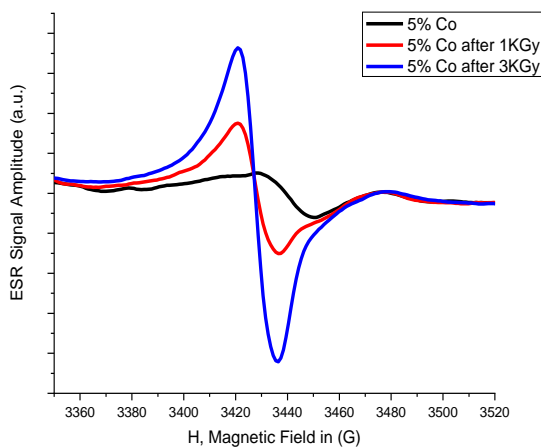


**Fig. (11):** ESR signal for 5% Co doped ZnO samples before and after irradiated with 1KGy and 3KGy doses.

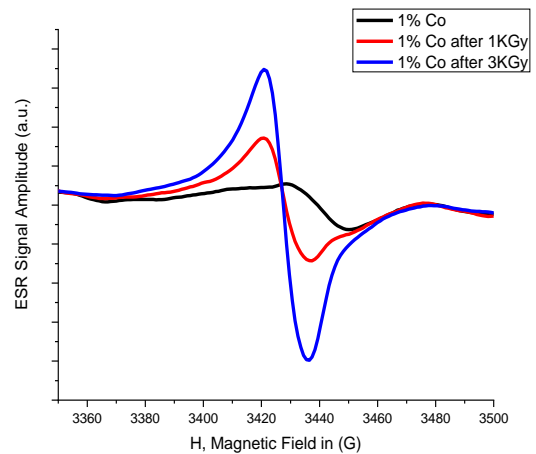


**Fig. (12):** ESR signal for 10% Co doped ZnO samples before and after irradiated with 1KGy and 3KGy doses.

#### 4. CONCLUSION

In this work, a successful deposition of pure and Co-doped ZnO thin films is reported. The Co-concentration in the obtained films was controlled by changing the amount of the cobalt source salt in the starting precursor. according to the XRD results, the preferred orientation of the deposited film was changes from (002) to (100) as the Co-content in the films increases. The bandgap also shows random response to the Co-content. The ESR analysis confirmed the presence of Co ions in the Co-

doped ZnO samples. The obtained ESR broad signal is strongly dependent on the increase of both Co concentrations and gamma-ray dose.

Co-doped ZnO thin films may be a good candidate for suitable application in various optoelectronic devices such as the manufacture of solar cells. Also, it is observed that pure ZnO shows a weak ferromagnetic nature whereas Co-doped thin films exhibit good ferromagnetic properties, which is used in the field of spintronic applications.

## 5. REFERENCES

- [1] Wolf, S.A., Lu, J., Stan, M.R., Chen, E., Treger, D.M.: The promise of nanomagnetic and spintronics for future logic and universal memory. *Proc. IEEE* 98(12), 2155–2168 (2010).
- [2] Liu, E.: Materials and designs of magnetic tunnel junctions with perpendicular magnetic anisotropy for high-density memory applications. Ph.D. thesis, Katholieke Universities Leuven, Belgium (2018)
- [3] Yakout, S.M.: Spintronics: future technology for new data storage and communication devices. *J. Supercond. Novel Magn.* (2020).
- [4] Kim, J., Paul, A., Crowell, P.A., Koester, S.J., Sapatnekar, S.S., Wang, J.-P., Kim, C.H.: Spin-based computing: device concepts, current status, and a case study on a high-performance microprocessor. *Proc. IEEE* 103(1), 106–130 (2014).
- [5] Banerjee, S. and A. Tyagi, *Functional materials: preparation, processing and applications*. 2011: Elsevier.
- [6] Hong, T., et al., Efficient photoelectrochemical water splitting over  $\text{Co}_3\text{O}_4$  and  $\text{Co}_3\text{O}_4/\text{Ag}$  composite structure. *Applied Catalysis B: Environmental*, 2017. 202: p. 454-459.
- [7] Steinfeld, A., S. Sanders, and R. Palumbo, Design aspects of solar thermochemical engineering—a case study: two-step water-splitting cycle using the  $\text{Fe}_3\text{O}_4/\text{FeO}$  redox system. *Solar Energy*, 1999. 65(1): p. 43-53.
- [8] Shaban, M., K. Abdelkarem, and A.M. El Sayed, Structural, optical and gas sensing properties of  $\text{Cu}_2\text{O}/\text{CuO}$  mixed phase: effect of the number of coated layers and (Cr+ S) co-Doping. *Phase Transitions*, 2019. 92(4): p. 347-359.
- [9] Kobayashi, R., et al., A heterojunction photocatalyst composed of zinc rhodium oxide, single crystal-derived bismuth vanadium oxide, and silver for overall pure-water splitting under visible light up to 740 nm. *Physical Chemistry Chemical Physics*, 2016. 18(40): p. 27754-27760.
- [10] Ahmed, A.M., et al., Enhanced photoelectrochemical water splitting activity of carbon nanotubes@  $\text{TiO}_2$  nanoribbons in different electrolytes. *Chemosphere*, 2020. 238: p. 124554.
- [11] Hensel, J., et al., Synergistic effect of CdSe quantum dot sensitization and nitrogen doping of  $\text{TiO}_2$  nanostructures for photoelectrochemical solar hydrogen generation. *Nano letters*, 2010. 10(2): p. 478-483.
- [12] Samir Hamrit, et.al. "Realization of high transparent conductive vanadium-doped zinc oxide thin films onto flexible PEN substrates by RF-magnetron sputtering using nanopowders targets," *Ceramics international*, Vol. 47, 2021, PP. 22881-22888.
- [13] N. Abirami, et.al., " Structural and magnetic properties of cobalt doped ZnO thin films deposited by cost effective nebulizer spray pyrolysis technique," *Material Research Express*, Vol. 7, 2020, PP. 1-12.
- [14] Awais Khalid, et.al., " Enhanced Optical and Antibacterial Activity of Hydrothermally Synthesized Cobalt-Doped Zinc Oxide Cylindrical Microcrystals," *Materials*, 2021, Vol. 14, PP. 1-16.
- [15] A. Abdel-Galil, M. R. Balboul, and A. Sharaf," synthesis and characterization of Mn-doped ZnO diluted magnetic semiconductors," *Physica B: Vol.* 477, 2015, PP: 20-28.
- [16] Desai, M.A., et al., Zinc oxide superstructures: Recent synthesis approaches and application for hydrogen production via photoelectrochemical water splitting. *International Journal of Hydrogen Energy*, 2018.
- [17] Aboud, A.A., M. Shaban, and N. Revaprasadu, Effect of Cu, Ni and Pb doping on the photoelectrochemical activity of ZnO thin films. *RSC Advances*, 2019. 9(14): p. 7729-7736.
- [18] Liu, M., et al., Enhancing water splitting activity and chemical stability of zinc oxide nanowire photoanodes with ultrathin titania shells. *The Journal of Physical Chemistry C*, 2013. 117(26): p. 13396-13402.
- [19] Tarwal, N., et al., A selective ethanol gas sensor based on spray-derived Ag–ZnO thin films. *Journal of materials science*, 2013. 48(20): p. 7274-7282.
- [20] Karzazi, O., et al., Structural, optical and magnetic properties of pulsed laser deposited Co-doped ZnO films. *Journal of Magnetism and Magnetic Materials*, 2015. 395: p. 28-33.
- [21] Ohyama, M., H. Kouzuka, and T. Yoko, Sol-gel preparation of ZnO films with extremely preferred orientation along (002) plane from zinc acetate solution. *Thin solid films*, 1997. 306(1): p. 78-85.
- [22] Benramache, S., B. Benhaoua, and O. Belahssen, The crystalline structure, conductivity and optical

- properties of Co-doped ZnO thin films. *Optik*, 2014. 125(19): p. 5864-5868.
- [23] Shukla, P., et al., Investigation on structural, morphological and optical properties of Co-doped ZnO thin films. *Physica B: Condensed Matter*, 2018. 550: p. 303-310.
- [24] Novák, P., et al. Self-texture control of ZnO films prepared by reactive RF magnetron sputtering. in *Key Engineering Materials*. 2014. Trans Tech Publ.
- [25] Srinivasulu, T., K. Saritha, and K.R. Reddy, Synthesis and characterization of Fe-doped ZnO thin films deposited by chemical spray pyrolysis. *Modern Electronic Materials*, 2017. 3(2): p. 76-85.
- [26] Hada, T., K. Wasa, and S. Hayakawa, Structures and electrical properties of zinc oxide films prepared by low pressure sputtering system. *Thin Solid Films*, 1971. 7(2): p. 135-145.
- [27] Aboud, A.A., et al., Characterization of nanocrystalline Co-La mixed oxide thin films prepared by the spray pyrolysis technique. *Results in Physics*, 2019. 12: p. 1513-1519.
- [28] Al-Gaashani, R., et al., XPS and optical studies of different morphologies of ZnO nanostructures prepared by microwave methods. *Ceramics International*, 2013. 39(3): p. 2283-2292.
- [29] Wang, C., et al., Role of cobalt in room-temperature ferromagnetic Co-doped ZnO thin films. *AIP Advances*, 2012. 2(1): p. 012182.
- [30] Kwoka, M., et al., Surface properties of nanostructured, porous ZnO thin films prepared by direct current reactive magnetron sputtering. *Materials*, 2018. 11(1): p. 131.
- [31] Yao, P.-C., S.-T. Hang, and M.-J. Wu, Growth characteristics and properties of Al-doped ZnO thin films by DC magnetron sputtering from AZOY@ target. *Transactions of the Canadian Society for Mechanical Engineering*, 2013. 37(3): p. 303-312.
- [32] Kodigala, S.R., Thin film solar cells from earth abundant materials: growth and characterization of Cu<sub>2</sub> (ZnSn)(SSe) 4 thin films and their solar cells. 2013: Newnes.
- [33] Li, G., et al., Structure and properties of Co-doped ZnO films prepared by thermal oxidization under a high magnetic field. *Nanoscale research letters*, 2015. 10(1): p. 1-8.
- [34] Li, W., et al., Tunable zinc interstitial related defects in ZnMgO and ZnCdO films. *Journal of Applied Physics*, 2015. 117(14): p. 145301.
- [35] Awan, S.U., et al., Effects of substitutional Li on the ferromagnetic response of Li co-doped ZnO: Co nanoparticles. *Journal of Physics: Condensed Matter*, 2013. 25(15): p. 156005.
- [36] Lee, H.-J., et al., Study of diluted magnetic semiconductor: Co-doped ZnO. *Applied Physics Letters*, 2002. 81(21): p. 4020-4022.
- [37] Wagner, C., et al., *Handbook of X-ray photoelectron spectroscopy*, Perkin-Elmer Corp. Eden Prairie, MN, 1979: p. 38.
- [38] Greczynski, G. and L. Hultman, In-situ observation of self-cleansing phenomena during ultra-high vacuum anneal of transition metal nitride thin films: Prospects for non-destructive photoelectron spectroscopy. *Applied Physics Letters*, 2016. 109(21): p. 211602.
- [39] Song, C., et al., The magnetic properties of Co-doped ZnO diluted magnetic insulator films prepared by direct current reactive magnetron co-sputtering. *Journal of magnetism and magnetic materials*, 2007. 309(1): p. 25-30.
- [40] Gungor, E., et al., Co doping induced structural and optical properties of sol-gel prepared ZnO thin films. *Applied Surface Science*, 2014. 318: p. 309-313.
- [41] Ivill, M., et al., Structure and magnetism of cobalt-doped ZnO thin films. *New Journal of Physics*, 2008. 10(6): p. 065002.
- [42] Tuan, A.C., et al., Epitaxial growth and properties of cobalt-doped ZnO on  $\alpha$ -Al<sub>2</sub>O<sub>3</sub> single-crystal substrates. *Physical Review B*, 2004. 70(5): p. 054424.
- [43] El-Naggar, A., S. El-Zaiat, and S.M. Hassan, Optical parameters of epitaxial GaN thin film on Si substrate from the reflection spectrum. *Optics & Laser Technology*, 2009. 41(3): p. 334-338.
- [44] Yusoff, N., et al., Core-shell Fe<sub>3</sub>O<sub>4</sub>-ZnO nanoparticles decorated on reduced graphene oxide for enhanced photoelectrochemical water splitting. *Ceramics International*, 2015. 41(3): p. 5117-5128.
- [45] Zhan, X., et al., Composition-Tuned ZnO/Zn x Cd<sub>1-x</sub> Te Core/Shell Nanowires Array with Broad Spectral Absorption from UV to NIR for Hydrogen

- Generation. ACS applied materials & interfaces, 2014. 6(4): p. 2878-2883.
- [46] Zhang, X., Y. Liu, and Z. Kang, 3D branched ZnO nanowire arrays decorated with plasmonic Au nanoparticles for high-performance photoelectrochemical water splitting. ACS applied materials & interfaces, 2014. 6(6): p. 4480-4489.
- [47] Li, Q., et al., Facile and scalable synthesis of "Caterpillar-like" ZnO nanostructures with enhanced photoelectrochemical water-splitting effect. The Journal of Physical Chemistry C, 2014. 118(25): p. 13467-13475.
- [48] Wu, M., et al., In situ growth of matchlike ZnO/Au plasmonic heterostructure for enhanced photoelectrochemical water splitting. ACS applied materials & interfaces, 2014. 6(17): p. 15052-15060.
- [49] Qiu, Y., et al., Secondary branching and nitrogen doping of ZnO nanotetrapods: building a highly active network for photoelectrochemical water splitting. Nano letters, 2012. 12(1): p. 407-413.